# CFD ANALYSIS OF UPPER PLENUM FLOW FOR A SODIUM-COOLED SMALL MODULAR REACTOR

**A. Kraus and R. Hu**
Nuclear Engineering Division
Argonne National Laboratory
9700 S Cass Ave., Argonne, IL, 60439, USA
arkraus@anl.gov; rhu@anl.gov

## ABSTRACT

Upper plenum flow behavior is important for many operational and safety issues in sodium fast reactors. The Prototype Gen-IV Sodium Fast Reactor (PGSFR), a pool-type, 150 MWe output power design, was used as a reference case for a detailed characterization of upper plenum flow for normal operating conditions. Computational Fluid Dynamics (CFD) simulation was utilized with detailed geometric modeling of major structures. Core outlet conditions based on prior system-level calculations were mapped to approximate the outlet temperatures and flow rates for each core assembly. Core outlet flow was found to largely bypass the Upper Internal Structures (UIS). Flow curves over the shield and circulates within the pool before exiting the plenum. Cross-flows and temperatures were evaluated near the core outlet, leading to a proposed height for the core outlet thermocouples to ensure accurate assembly-specific temperature readings. A passive scalar was used to evaluate fluid residence time from core outlet to IHX inlet, which can be used to assess the applicability of various methods for monitoring fuel failure. Additionally, the gas entrainment likelihood was assessed based on the CFD simulation results. Based on the evaluation of velocity gradients and turbulent kinetic energies and the available gas entrainment criteria in the literature, simulation results suggest that significant gas entrainment is unlikely for the current PGSFR design.

**KEYWORDS**
sodium fast reactor, gas entrainment, computational fluid dynamics, upper plenum, UIS

## 1. INTRODUCTION

Sodium fast reactor (SFR) technology is very promising for closing the nuclear fuel cycle. As one of the reactor types emphasized in the Gen-IV initiative, future SFRs should display enhanced safety and better performance compared to currently operating reactors. A number of thermal hydraulic topics should be addressed for any prospective design [1] in order to enable this goal. Particularly, the upper plenum flow characteristics are of importance to a number of safety and operational issues during normal operating conditions. These notably include gas entrainment, instrumentation techniques and locations, and temperature feedback.

A reference design analyzed here is the Prototype Gen-IV Sodium Fast Reactor (PGSFR), currently being jointly developed by the Korea Atomic Energy Research Institute (KAERI) and Argonne National Laboratory (ANL). It is envisioned that this fast spectrum advanced burner reactor will be employed to consume transuranics as part of an advanced fuel cycle. The current PGSFR design concept specifies a 150 MWe liquid sodium-cooled fast reactor in a pool-type primary system configuration [2-5]. A significant amount of analysis has been performed concerning various performance and safety aspects of

the PGSFR [5], but a number of details remain to be investigated. The aspect investigated here is to characterize flow behavior during normal operation in the upper plenum.

The PGSFR is a standard double-pool design. In normal operation, hot sodium flow discharges from the core into the "hot" pool, the geometry of which is shown in Fig. 1. This pool contains shielding, four intermediate heat exchangers (IHXs), the in-vessel transfer machine (IVTM), and the upper internal structure (UIS), which contains the control rod driveline (CRDL) structures, thermocouples (TCs), and other instrumentation. The UIS has a "slot" that is utilized by the IVTM during fuel assembly shuffling, but is empty during normal operation. The sodium flow passes through the primary side of the IHXs and cools, discharging into the "cold" pool. From here it is pumped back through the core. The pools are completely separated from each other by a steel "redan" structure. An inert cover gas is present over both of the pools.

A number of phenomena relevant to reactor safety and performance need to be assessed through an understanding of the flow in the hot pool. The general splitting of flow to different regions of the pool is of interest, and any stagnant regions should be identified. Flow should be split nearly equally between the IHXs to provide for more even heat transfer, but given the asymmetry of some features, notably the placement of the UIS and IVTM, this is not certain. The amount of flow bypassing the UIS is also of interest. Some beneficial feedback mechanisms, such as expansion of the CRDLs, are dependent on temperature being convected by the coolant to specific areas. If there is little flow through the UIS, the impact of these feedback mechanisms will be significantly reduced.

Entrainment of the cover gas is another potential issue. Velocity, vorticity and turbulent kinetic energy (TKE) at the interface between the liquid sodium and the cover gas should be kept to reasonably low values. As velocity at this interface increases, significant gas entrainment (GE) into the sodium becomes increasingly likely. This can degrade the thermal performance of the coolant as well as introduce potential reactivity effects. Significant entrainment could also reduce pump efficiency. While it can be mitigated through use of perforated plates and other devices [6], these introduce additional complexity and cost to the design. Hence it is worthwhile to estimate the risk of entrainment for the base design.

Upper plenum flow characterization can also aid in determining measurement techniques and locations. Accurate readings of the outlet temperature of each assembly are very important for identifying the location of any potential core issues. Hence the TCs must be close enough to the core that little mixing between assembly outlets has occurred. It is also beneficial from a structural standpoint to have the TCs as far from the core outlet as is reasonable. Thus a balance between these two needs must be maintained. The residence time of the sodium in the upper plenum could also be important for measurement techniques for detecting fuel failures. Establishing the average residence time would help to decide which potential detection methods and locations are appropriate.

Upper plenum flow studies have previously been undertaken by other authors. Shibahara et al. [7] and Mochizuki and Yao [8] have performed computational fluid dynamics (CFD) analysis of the "Monju" (loop-type) reactor. This reactor features a similar flow-path to that in the PGSFR, notably flow impinging on a large resistance and curving over a walled section. However, their primary focus was thermal stratification, and there are no results for gas entrainment or residence time. Banerjee et al. [9] provided CFD results for gas entrainment mitigation, but the reactor investigated features the opposite circulation direction compared to PGSFR. Since gas entrainment is also strongly influenced by geometry, it is doubtful that these results would generalize well to the PGSFR design. This is of particular concern in the IVTM and slot vicinities.

## 2. METHODS

### 2.1. Geometry and Meshing

To assess the detailed flow patterns in the hot pool, CFD analysis is performed with explicit modeling of the geometries of the various structures in the UIS (Fig. 2). The commercial code STAR-CCM+, a general-purpose CFD and multi-physics code based on the finite volume method, was employed in this work [10]. The TC bundle housing and CRDL tubes were assumed to be solid for this analysis. The slot portion of the UIS is used during refueling operations, but is empty during normal operation. The boundaries of the inner core and reflector zone outlets, i.e. the flow inlets to the domain, were approximated as circles with the equivalent radii of their respective hexagonal zones. These were separated by a small wall in order to have different inlet conditions for the two zones. The top of the fluid was bounded by the prescribed height of the hot sodium during normal operation. Since only the flow in the hot pool is of interest here, the computational domain outlets were constructed by extruding downward within the IHX inner shell to a distance such that no reversed flow occurred.

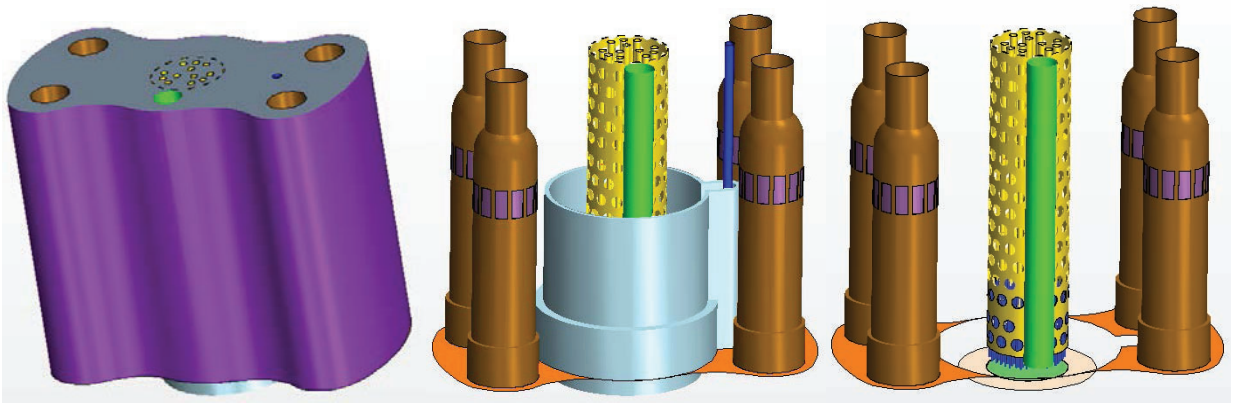

**Figure 1. PGSFR geometry, with redan surface (purple and orange), sodium-gas interface (gray), UIS (yellow), IVTM (green), shield (steel), IHXs (brown), core outlet (green circle) and reflector outlet (tan).**

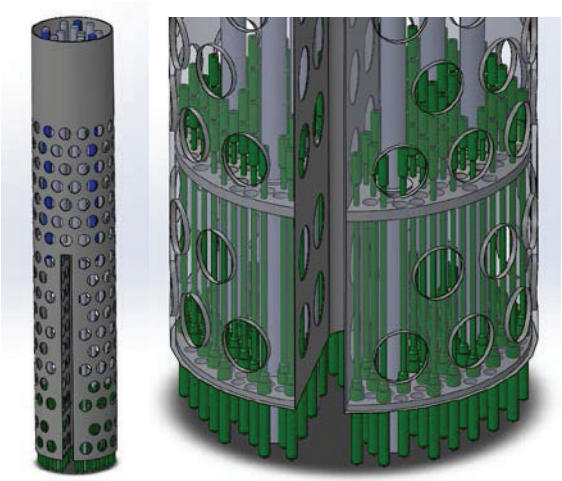

**Figure 2. UIS CAD structure (provided by KAERI), clearly showing slot and orifice plates. Green structures are TCs, blue are TC wire bundle housings, and gray cylinders are CRDLs.**

Meshes for this geometry were built with primarily polyhedral cells. A layer of prismatic cells was generated at all walls for more accurate modeling of near-wall turbulence. The layer was tailored such that in most areas, the y+ value for the wall cell was greater than 20 but less than 200. In some cases, a small number of wall cells exceeded this value. Multiple computational meshes were tested, ranging from ~3 million cells (the "coarse" mesh) to ~45 million cells (the "fine" mesh). Sample cross-sectional views of these meshes can be found in Fig. 3. A relatively fine mesh was necessary at the core exit in the vicinity of the TCs to capture the flow behavior well in this area, as well as the spatial variation in the inlet conditions. The general characteristics of the flow were similar for all meshes. The fine mesh case was more appropriate, particularly for high resolution of the core outlet and TC area, but carried an increased computational cost.

### 2.2. Physical and Numerical Modeling

The areas between the IHX windows and the actual domain outlets were treated as porous media. Since flow details in the IHXs are not important for this simulation, resistance coefficients were selected such that the pressure drop roughly matched that from prior 1-D SAS4A/SASSYS-1 system code [11-12] simulations. Early simulations without the porous media displayed unstable outlet flow partitioning, which was thought to be due to the minimal frictional losses in the domain. Thus the momentum sink of the porous media has a stabilizing effect on the computation, but is realistic since there is significant resistance due to IHX internals.

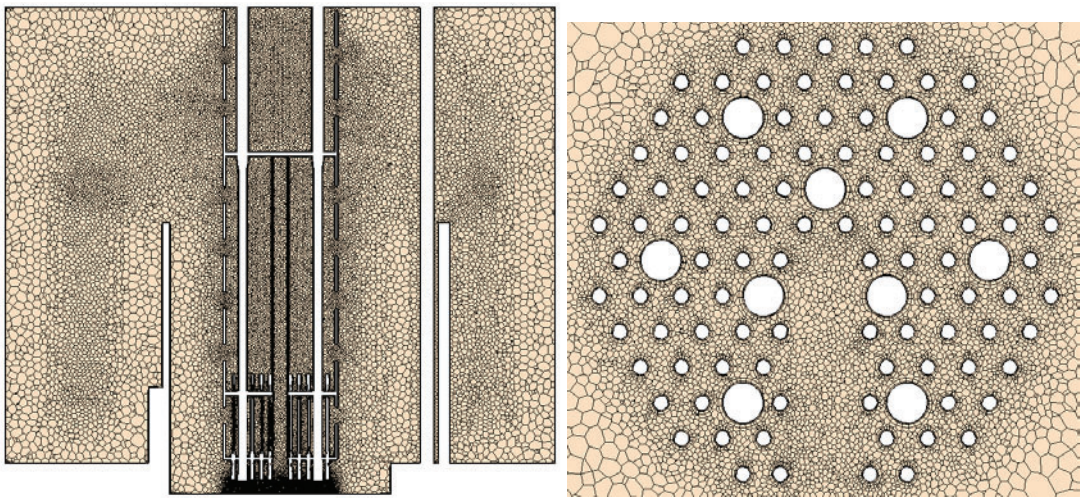

**Figure 3. Coarse mesh planar views at domain midplane (left, front view) and zoomed in at TC area (right, top view).**

Turbulence was modeled with the k-ω SST model [13] using an "All-y+" adaptive wall modeling approach. Buoyancy was not modeled due to the relatively low temperature difference between the assemblies and the strength of the jets in the core outlet vicinity. The minimum jet Froude number was 55, which gave justification for neglecting buoyancy. Constant thermal properties were used [14]. Second-order schemes were used for all convective terms. Both steady Reynolds-Averaged Navier-Stokes (RANS) and unsteady (URANS) calculations were performed.

A passive scalar model was activated to obtain the fluid residence time. Values were reported on a cell-by-cell basis to establish a frequency distribution for the residence time from the core outlet to IHX inlets, given the number of potential flow paths through the IHX windows. An average was taken over these values to establish an expected flow time from the core to the IHX outlets.

### 2.3. Boundary Conditions

The boundary condition (BC) at the sodium-cover gas interface was assumed to be a slip wall in this work. This essentially assumes that the velocities of the liquid and gas are equal at a given point of the interface. This is a compromise between accuracy, simulation time, and complexity. More accurate results could in theory be obtained with a volume-of-fluid (VOF) multiphase simulation, where the interface is tracked and entrainment could be directly simulated. However, the VOF simulation would require a much finer mesh, and is only available for URANS simulations. Time steps and mesh refinements necessary for a volume of this size would result in impractical simulation times. Thus the slip approximation was deemed acceptable at this stage. Higher-fidelity modeling could be performed in future work.

No-slip and adiabatic conditions were enforced at all physical walls. Pressure outlet conditions were used such that the outlet pressure of each IHX was the same. Velocity inlet boundaries were used for both the inner core and reflector, although flow emerging from the reflector is so low as to be nearly stagnant. In order to model the core outlet conditions in a realistic fashion, a detailed approach was needed.

Instead of attempting to create core outlet geometry at the CAD level, where any changes would require re-meshing and further adaptation of the simulation setup, the core outlet conditions were imposed on the computational mesh directly through user code. Routines were written in C to map velocity and temperature profiles for the inlet based on the cell face centroids in that area. These routines were compiled into a library and imported into STAR-CCM+. Any changes in the modeling approach could thus be incorporated through changing the user library, without any need for recreating the CAD model or the computational mesh.

Data for the core outlet conditions was obtained from prior design analyses of the PGSFR [12]. These conditions were used to map the flow rate and outlet temperature for each individual fuel assembly location in the core. The results of this mapping are shown in Fig. 4. To maintain the flow rate and attempt to match the average velocity, the flow area of the assembly was calculated as the area of the interior of its hexagonal can minus that of 217 wire-wrapped pins. For mapping simplicity, this area was approximated as a circle centered at the assembly center. All non-assembly positions, including control assemblies due to their comparatively low flow, were assigned zero-velocity and core-average-temperature (818 K) values. The detailed mapping procedure was not applied to the reflector region, given its very low flow. Plug velocity and turbulence profiles were used for each assembly. These are only expected to give a rough approximation of the assembly outlet conditions, as no detailed simulation data of these conditions was available.

### 2.4. Gas Entrainment Evaluation Approach

A number of factors near the free surface influence GE, including downward velocity, velocity gradient, and vorticity. One method, based on Sakai et al. [15], is to compute a non-dimensional downward velocity gradient based on the ratio of viscous to gravity forces:

$$\alpha^* = \frac{\alpha \nu}{gh} \tag{1}$$

where h is the height between the free surface and the outlet, α is the velocity gradient in the downward direction, g is the gravitational constant, and ν is the kinematic viscosity. The value of h was selected to be the distance from the free surface to the IHX inlet window centerpoint. This is a conservative value. If the "outlet" is taken to be the IHX outlet, then $\alpha^*$ is ~3 times lower. However, this $\alpha^*$ correlation is for a "bathtub" vortex leading directly to the outlet itself, and the situation here is more complex given the geometry change when entering the IHX. The limiting value for bubble detachment is $1.0 * 10^{-7}$ based on Eq. 1 [15]. In this work, vertical velocity gradients were taken from the cell-centered values of cells at the top surface, as gradients at the wall itself are defined as zero.

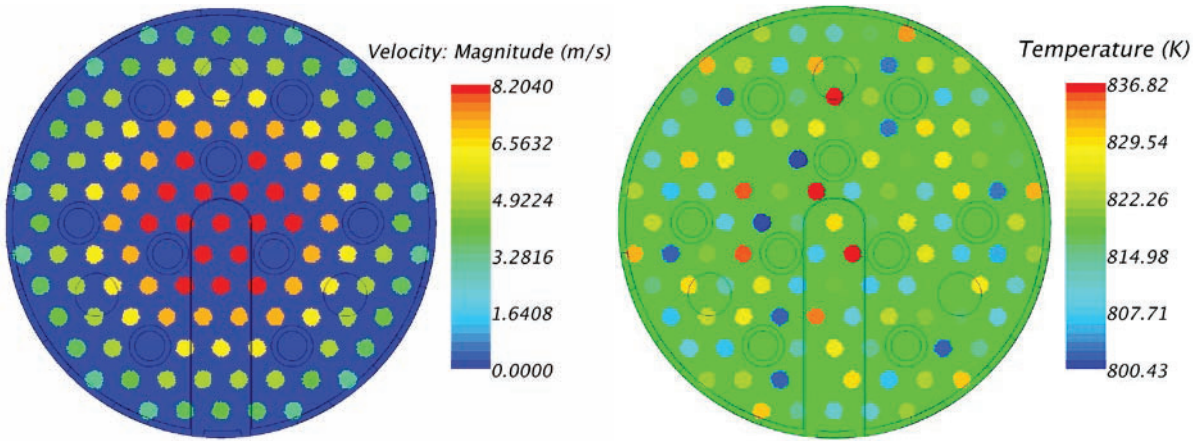


**Figure 4. Velocity (L) and temperature (R) inlet conditions with assembly-by-assembly mapping, with UIS structures overlaid for reference.**

There are also other ways entrainment can occur, such as from sloshing liquid trapping gas pockets, as investigated in Mali and Patwardhan [16]. Mali states that "the process of gas entrainment cannot be characterized in terms of the peak shear velocity," and that more is required. They looked at turbulent kinetic energy (TKE) at the surface and found that "the values of turbulent kinetic energy at the onset of gas entrainment are similar over a wide range of geometry and operating conditions" and that TKE was the "major parameter that governs the onset of gas entrainment". Also shown was that higher TKE is required for higher surface tension fluids, so the required TKE for sodium would be roughly 3 times higher than for water. Hence TKE values in the range of 0.18 $m^2/s^2$ or more would likely be necessary at the top surface for entrainment due to sloshing.

Gas entrainment is a complex phenomenon which can be difficult to correlate. Literature review has shown that entrainment is very geometry-dependent, so adaptability to the current design should be treated with care. Additionally, many experimental data are for water. Sodium has a surface tension roughly three times higher than water, which will reduce entrainment likelihood. Resolution of individual vortices may not be achievable given the size of the volume. For these reasons the purpose of the GE approach here is to provide an estimate of where problematic areas may be and the general severity of any potential entrainment.

## 3. RESULTS AND DISCUSSION

### 3.1. Evaluation Methods for Simulation Results

Simulation results were assessed in a number of ways to investigate convergence and obtain values of interest. These included standard residual-based convergence, where $10^{-4}$ is a typical (normalized)

reference value for a convergent equation. Average and maximum values on various surfaces of the domain of flow parameters such as velocity were recorded to compare their convergence iteration by iteration. This was also performed for point probes at various cells, notably near the core outlet in order to assess the temperatures near the TCs. For the URANS simulations, these values were compared over time in an attempt to establish whether or not the oscillations were periodic in nature.

Steady simulations yielded subpar residual convergence for all of the cases that were run. The other monitors, e.g. mass flow splitting between the four outlets, did not settle to any one value, as shown in Fig. 5. For these reasons, unsteady simulations were also performed, which displayed good residual convergence. For the unsteady simulations, the total mass flow rate is converged from about 18000 iterations onward (the point at which the simulation was "restarted" with an unsteady approach), which is the period over which field statistics were taken. The changes in flow rates over the nearly 160s simulated are only on the order of 2 kg/s, or 0.4% of the mean value.

Statistics were gathered over time to establish the mean and variance of flow parameters. Many of the point probes in various sections of the domain, however, did not show any periodic behavior over the time simulated. Some flow parameters and domain areas showed greater variability than others. Hence there could be some numerical instability present. Efforts to mitigate this, including improving mesh refinement and quality, time step and solver tolerance changes, etc., are ongoing. That said, the majority of flow structures and behavior were consistent between runs, and made sense from a physical perspective. For these reasons, it is the authors' view that the following results can be used to gauge the general flow behavior in the hot pool, with the caveat that some of the isolated values may not be exact.

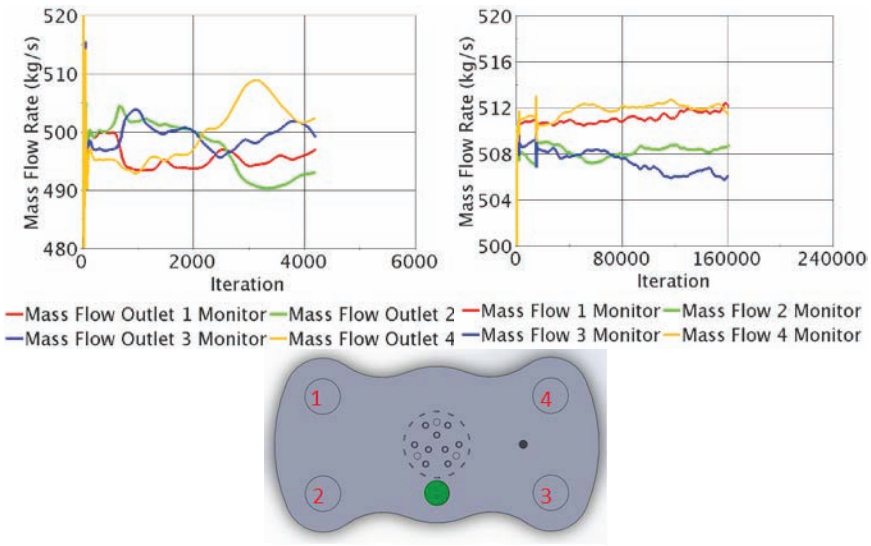


**Figure 5. Mass flow splitting between the outlets by iteration. Monitors as labeled above, where green is the IVTM. Both steady fine-mesh (L) and unsteady coarse-mesh (R) results are shown.**

### 3.2. General Flow Behavior

Figs. 6-8 display the general flow patterns and behavior in the hot pool. Flow in the TC area and the rest of the UIS is largely symmetric. Velocity from the core outlet jets is high but dissipates rather quickly as it is pushed to the shield region. The UIS orifice plate clearly provides strong resistance to the flow, as much of the flow dramatically curves around the UIS and bypasses it entirely. Mass flow at the bottom of the UIS is split in portions of 34.5% into the UIS orifice plate, 24.7% to the slot area, and 40.8% into the

bypass flow. Hence there is relatively low flow through the UIS except when also considering the slot area, which offers minimal resistance and has high coolant velocity. Flow exits the slot either by flowing out around the IVTM or by leaving through the UIS holes. Some of the flow going toward the IVTM follows parallel to it all the way to the top of the domain.

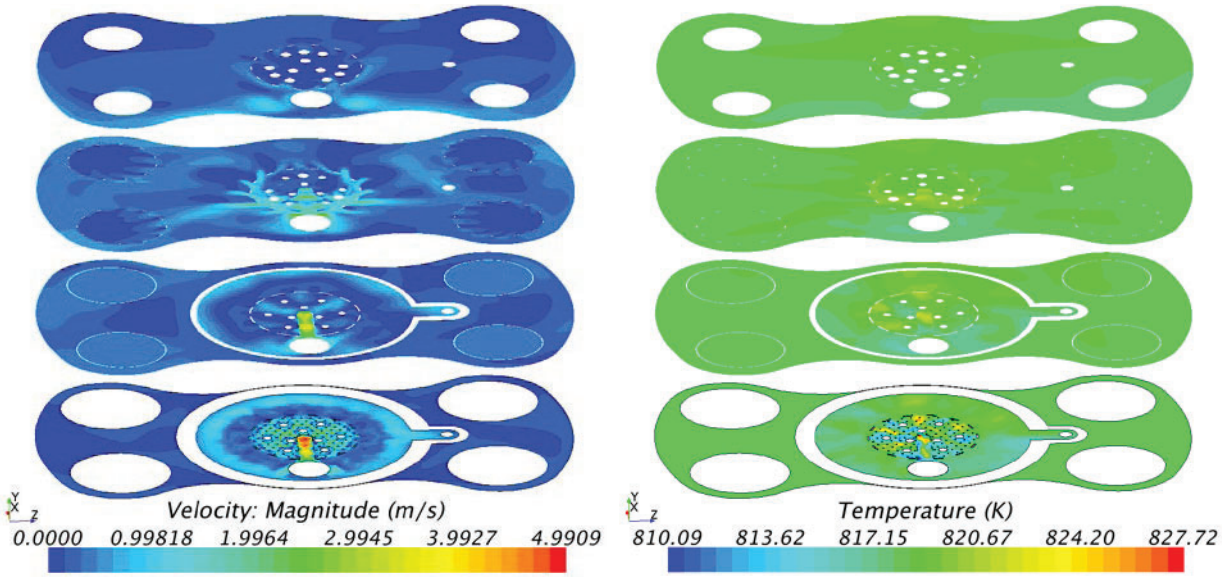


**Figure 6. Velocity magnitude (left) and temperature (right) at planes of height 0.2m, 2.2m, 4.2m, and 6.2m. Height of 0m corresponds to the redan base. UIS has generally warmer fluid than surrounding area.**

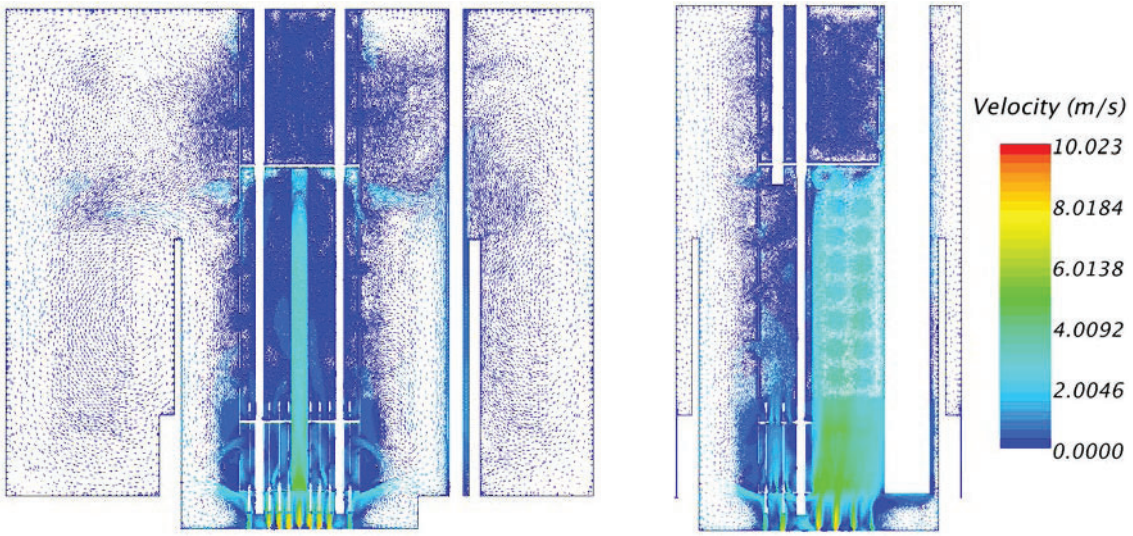


**Figure 7. Velocity vectors in the Y-Z (left) and X-Y (right) planes. For X-Y, IVTM and UIS slot are on the right side.**

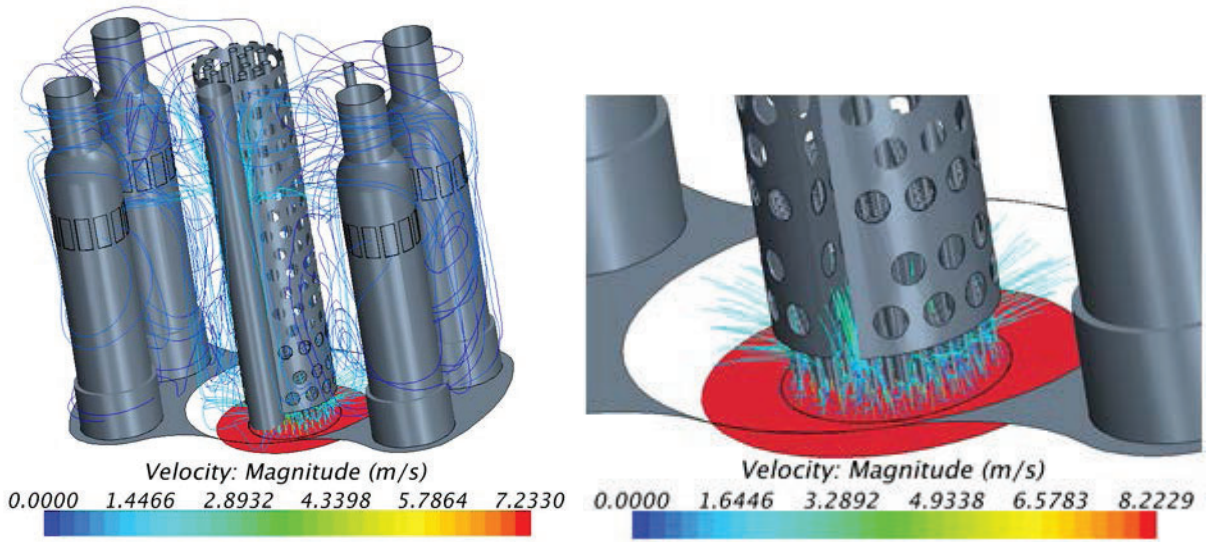


**Figure 8. Streamlines for the hot pool. Most streamlines spread around UIS or go to the slot area, curve over the shield and the top of the IHXs, and recirculate before entering the IHXs.**

Despite having a lower proportion of the total flow than the bypass, the flow that does go into the UIS region is relatively higher in temperature than the flow outside of it. This may be due to the slot lying above some of the hotter outlets, and dispersing some of this hot fluid to the rest of the UIS. This could prove beneficial for the reactivity feedback due to CRDL expansion via convective heating. This is of course dependent on the final slot alignment with respect to peak temperatures (see Section 2.3). While conduction through the redan is not modeled, its effects on temperatures in areas of interest for this simulation should be minimal. The jets from the core are also strong enough that the redan conduction should not affect TC readings or the temperature distribution within the UIS.

The flow pattern in the PGSFR upper plenum is complex, and large circulations were observed. It was observed that there are low velocity regions in the upper plenum, but no really stagnant regions. For the lowest velocity region (lower part of the narrow gap between the shield and redan wall), the average flow velocity was 0.074 m/s. Flow that bypasses the UIS stays close to the shield wall before emerging. The relatively high coolant velocity, combined with the IHX windows and the top of the shield being of similar height, forces the coolant to take an arcing path upon exiting the shield region. The curvature of this path is such that the majority of the flow goes over the top of the IHX and enters each IHX on the side furthest from the core. While the mass flow split displayed some oscillation during the calculations, flow was not strongly inclined towards any particular outlet. There was less than 5% difference between the lowest and highest IHX mass flow rates at any given time.

### 3.3. Thermocouple Positioning

Temperatures and normalized cross-velocities were recorded for each assembly from the core outlet to 0.2m above. These clearly show that many of the assemblies display a strong cross-velocity, which enhances mixing. Temperature changes were normalized to the maximum outlet temperature difference of all assemblies (36.4 K). The maximum change of 5.9% (~2 K) was at one of the outer assemblies (Fig. 9-10), where dispersal away from the UIS occurs quickly. 91 of the 112 assemblies, however, had normalized changes of less than 1%. Based on the axial development, putting the TCs ~0.1 m above the core outlet would yield temperatures almost identical to the outlet. If this is simple enough to do from a structural standpoint, it should be considered. The cross flow velocity should also be considered. With the TCs located 0.2 m above the core outlet, flow at some TC locations experienced strong cross flow (over

15%). If the distance is reduced to 0.1 m above the core outlet, cross flow at most TC locations would be less than 5%.

It is important to note, however, that these values are only one reference case. Since the core geometry is 1/3-symmetric, there are two other viable orientations for the same core data. If the UIS were itself also 1/3-symmetric then mixing results would likely be similar for all orientations, but the presence and positioning of the slot makes it 1/2-symmetric. As described in Section 3.2, this may have a significant impact on local mixing and on the temperature in the UIS regions. As seen in Fig. 9, except for some edge assemblies, all of the assemblies with 1% or greater normalized temperature change are in the vicinity of the slot. The data presented here are also for a full-flow case with high core outlet velocity, so buoyancy effects were neglected. For lower-flow conditions, as may be present in an accident scenario, buoyant mixing may need to be included for accurate modeling. If needed, some parametric studies could be performed to gauge the impact of the above with the final core outlet temperature distribution.

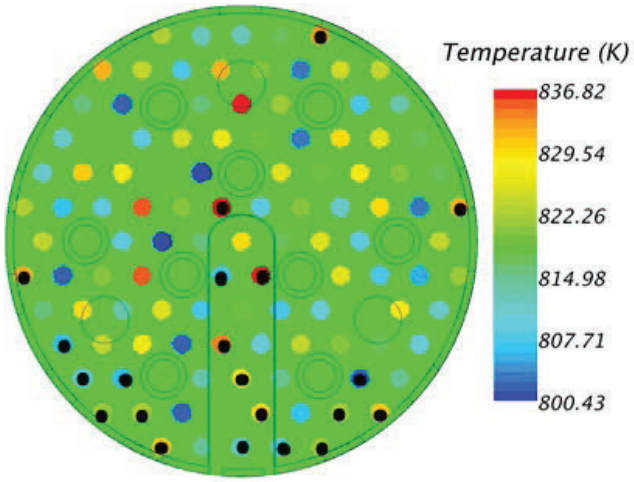


**Figure 9. Assembly locations with greater than 1% normalized temperature change, denoted by black dots. Excepting edge assemblies, the rest are all clearly influenced by the slot positioning.**

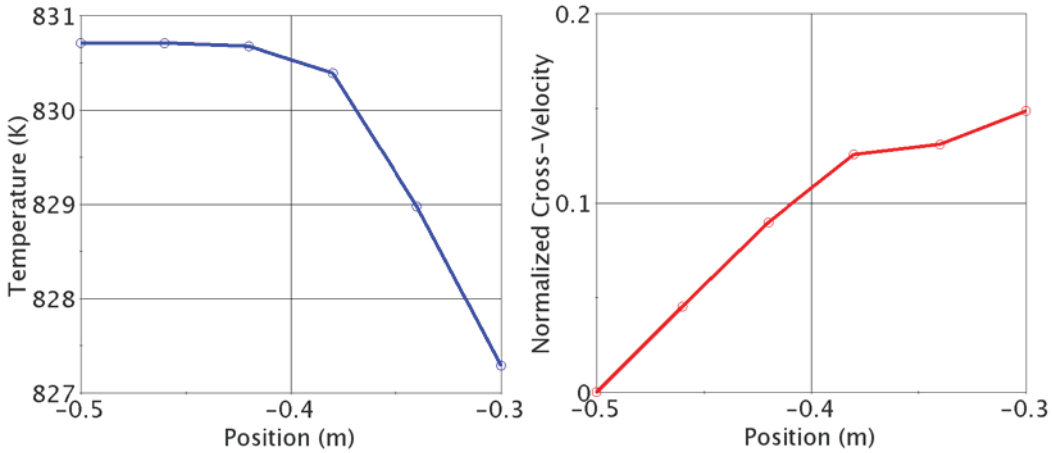


**Figure 10. Temperature (left) and normalized cross-velocity (right) for the assembly with the largest normalized temperature change.**

### 3.4. Gas Entrainment

Downward velocity gradients were found to be quite high in some areas of the slip wall (Fig. 11), notably at some "corners" where the slip wall meets the wall of another component (UIS, IVTM, etc.). The GE estimation method does not explicitly account for variations at walls as compared to isolated vortices. Moreover, the mesh resolution in some of these areas was such that only single localized cells had these high values. Thus GE evaluations were performed for both the simulated peak and "non-corner" peak values, which based on Eq. 1 in Section 2.4 were -12.5 $s^{-1}$ and roughly -3.0 $s^{-1}$, respectively. These yield corresponding $\alpha^*$ values of 1.3 * $10^{-7}$ and 0.3 * $10^{-7}$. If a different value for the height is used (see Section 2.4), the $\alpha^*$ values will be even lower.

As noted in Section 2.4, the limiting value for bubble detachment is 1.0 * $10^{-7}$ for the dimensionless downward velocity gradient [15]. Thus, this analysis indicates that there would likely only be GE in the peak "near-wall" areas. Some aspects of the simulation, however, indicate that this entrainment is unlikely to be a strong concern. As shown in Fig. 11, the magnitude of the downward velocity is very small near the sodium-gas interface. Furthermore, even if GE occurs near the UIS walls, it would be largely contained. The localization of the phenomenon also makes it easier to mitigate through use of plates or other devices.

Fig. 13 displays the TKE at the free surface. From [16], TKE values in the range of 0.18 $m^2/s^2$ or more would likely be necessary for gas entrainment by sloshing at the top surface, which is well above the peak found in this simulation (0.14 $m^2/s^2$), and would again be localized to similar areas as for the vortex-driven entrainment. So even considering the shearing of the gas-liquid interface, gas entrainment is unlikely for the current system setup, and can be mitigated in a straightforward manner using plates or baffles at a few strategic locations near the top of the UIS and IVTM.

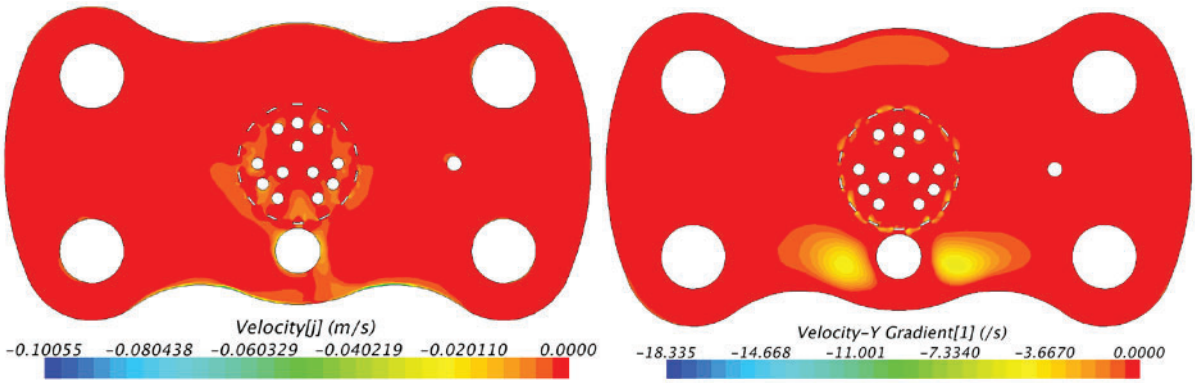


**Figure 11. Magnitude (left) and gradient (right) of axial velocity at the free surface. Peaks are due to interactions with IVTM/UIS. Positive values clipped to emphasize the downward values.**

### 3.5. Fluid Residence Time

Via passive scalar transport, it was found that the average residence time of the fluid in the upper plenum is about 64 seconds. Fig. 14 shows the frequency distribution of the residence time for each of the window cells for all four IHXs. Due to the strong curvature around the shield, flow typically circulates before entering the IHX, leading to longer residence times. There are a few cells with high residence times that are either due to more circulations or potentially flow through one IHX window and out another. These are very few in frequency, however, and the vast majority of flow should reach the IHX

inlet within two minutes. This residence time data could be used to evaluate potential methods for fuel failure detection. Many methods are dependent on decay of certain fission products being detected in the coolant, and if residence time is too long, this decay cannot be reliably detected.

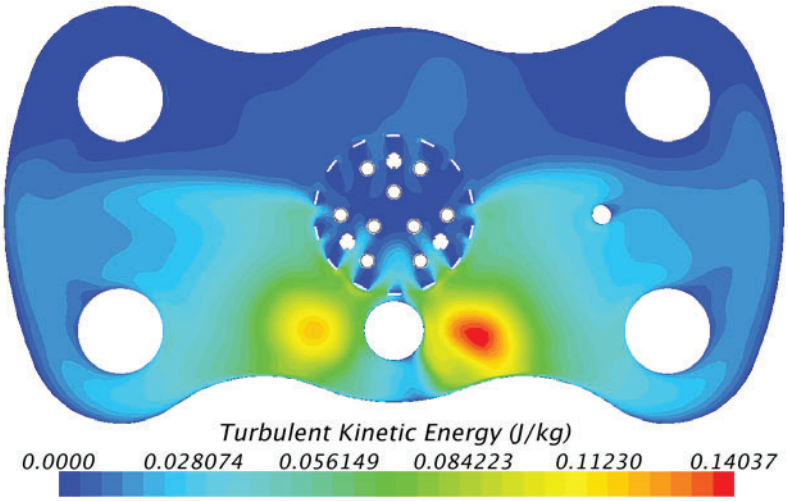


**Figure 12. Turbulent kinetic energy at the top surface.**

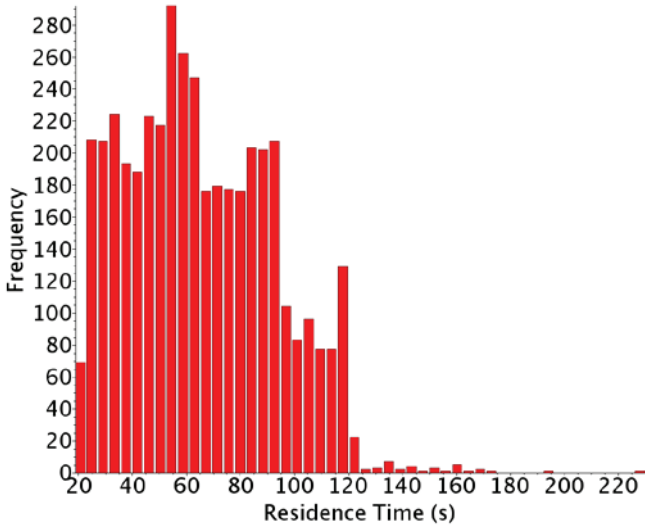


**Figure 13. Distribution of fluid residence time (s) from core outlet to IHX inlet.**

## 4. CONCLUSIONS AND FUTURE WORK

The detailed flow pattern in the upper plenum of an SFR is of significant importance to a number of safety and operational issues. A detailed CFD analysis of the velocity and temperature fields in the hot pool of PGSFR has been performed during normal operation conditions. The predominant flow patterns have been established. The temperature mixing near the TCs has been assessed and while most assemblies should have fairly representative temperature readings, it was found that if they were located less than 0.1m above the core outlet, readings would be nearly identical to the outlet. Additionally, gas entrainment was estimated to be unlikely due to bubble detachment at the sodium-gas interface. Even if it were to

occur, it would likely be minimal and localized in such a way as to be easily mitigated. Fluid residence time was found to have a reasonably wide range of potential values, with a mean time of 64 s. This time can be used to evaluate potential fuel failure detection methods.

The complicated flow characteristics in the upper plenum suggest topics of interest for future studies. First, simulations with abnormal flow rate and temperature of one subassembly outlet (due to flow blockage) would be of interest to further assess the core outlet temperature measurement strategy. Second, the control rod drive line expansion is an important reactivity feedback mechanism for PGSFR safety during design basis accidents or design extended conditions. It would be beneficial to perform CFD analyses to study the temperature response of the CRDLs during abnormal core outlet (flow and temperature) conditions. Third, coupled system and CFD code simulation of PGSFR transients would be necessary to examine the thermal stratification in the hot and cold pools, and to assure reactor safety during transition to natural circulation cooling. Finally, the results from the current work can better inform appropriate flow boundary conditions for future detailed modeling of gas entrainment behavior at the sodium-gas interface.

## ACKNOWLEDGMENTS

The authors would like to thank KAERI for providing the hot pool drawings, the UIS CAD model, and frequent feedback. The authors would also like to thank Florent Heidet and Anton Moisseytev for providing core outlet boundary conditions. This work was supported by Korea Atomic Energy Research Institute under the Work-for-Others Agreement No. 85E20: KAERI-ANL Joint Program on Design Development of a Prototype Sodium-cooled Fast Reactor. The submitted manuscript has been created by UChicago Argonne, LLC, Operator of Argonne National Laboratory (“Argonne”). Argonne, a U.S. Department of Energy Office of Science laboratory, is operated under Contract No. DE-AC02-06CH11357. The U.S. Government retains for itself, and others acting on its behalf, a paid-up nonexclusive, irrevocable worldwide license in said article to reproduce, prepare derivative works, distribute copies to the public, and perform publicly and display publicly, by or on behalf of the Government.

## REFERENCES

1. D. Tenchine, “Some Thermal Hydraulic Challenges in Sodium Cooled Fast Reactors,” *Nuc. Eng. Des.*, **240**, pp. 1195-1217 (2010).
2. D. Hartanto and Y. Kim, “Conceptual Study of a Long-Life Prototype Gen-IV Sodium-Cooled Fast Reactor (PGSFR),” *PHYSOR 2014*, Kyoto, Japan, Sep. 28-Oct. 3, on CD-ROM (2014).
3. A. Shin et al., “Development Status of TRACE Model for PGSFR Safety Evaluation,” *Korean Nuclear Society Spring Meeting*, Jeju, Korea, May 29-30, on CD-ROM (2014).
4. D. Kim, J. Eoh, and T.H. Lee, “An Optimal Design Approach for the Decay Heat Removal System in the PGSFR,” *ASME 4th Joint US-European Fluids Engineering Division Summer Meeting (FEDSM)*, Chicago, IL, USA, Aug. 3-7, on CD-ROM (2014).
5. A. Kraus and R. Hu, “CFD Simulation of Natural Convection Cooling After a Loss-of-Flow Transient,” *16th International Topical Meeting on Nuclear Reactor Thermal Hydraulics (NURETH-16)*, Chicago, IL, USA, Aug. 30-Sep. 4, 2015, on CD-ROM.
6. D. Tenchine, C. Fournier, and Y. Dolias, “Gas Entrainment Issues in Sodium Cooled Fast Reactors,” *Nuc. Eng. Des.*, **270**, pp. 302-311 (2014).
7. M. Shibahara, T. Takata, and A. Yamaguchi, “Numerical Study on Thermal Stratification Phenomena in Upper Plenum of LMFBR ‘MONJU’,” *Nuc. Eng. Des.*, **258**, pp. 226-234 (2013).
8. H. Mochizuki and H. Yao, “Analysis of Thermal Stratification in the Upper Plenum of the ‘Monju’ Reactor,” *Nuc. Eng. Des.*, **270**, pp. 48-59 (2014).

9. I. Banerjee et al., “Development of Gas Entrainment Mitigation Devices for PFBR Hot Pool,” *Nuc. Eng. Des.*, **258**, pp.258-265 (2013).
10. CD-Adapco, “STAR-CCM+ 9.04 Manual,” Melville, NY, 2014.
11. T. H. Fanning, ed., “The SAS4A/SASSYS-1 Safety Analysis Code System,” ANL/NE-12/4, Nuclear Engineering Division, Argonne National Laboratory, January 31, 2012.
12. F. Heidet and A. Moisseytev, Argonne National Laboratory, private communication, June 2014.
13. F.R. Menter, “Two-Equation Eddy-Viscosity Turbulence Models for Engineering Applications,” *AIAA J.*, **32**, pp. 1598-1605 (1992).
14. J.K. Fink and L. Leibowitz, “Thermodynamic and Transport Properties of Sodium Liquid and Vapor,” ANL/RE-95/2, Jan. 1995.
15. T. Sakai et al., “Proposal of Design Criteria for Gas Entrainment from Vortex Dimples Based on a Computational Fluid Dynamics Method,” *Heat Transfer Eng.*, **29**(8), pp. 731-739 (2008).
16. R. Mali and A. Patwardhan, “Characterization of Onset of Entrainment in Stirred Tanks,” *Chem. Eng. Res. Des.*, **87**, pp. 951-961 (2009).